Falcon-inspired Robotic Glider with Multi-joint Wing Morphing

Jonathan Ali, Karla Soto Cuevas, Kruti Rachapudi, Helen Wang, Tommii Zeng

***Abstract*—Current variable-sweep aerial designs predominantly feature one-joint wing systems to increase diving speed, while addressing concerns regarding vibration management and mechanical durability. By drawing inspiration from the double-joint sweep wing morphology of the peregrine falcon, the effects on vibration and speed during diving were studied. The purpose of this project is to test whether a two-joint variable-sweeping wing system that folds its outer wings towards the body during flight will increase diving speed and reduce vibrations in comparison to fixed-wing and one-joint variable-sweep wing systems. The results show that, while double-joint and single-joint wings exhibit higher average vibrations than fixed wings, the difference between the two variable-sweep designs is not statistically significant with a 95 percent confidence interval. However, double-joint wings achieve higher average speeds ($\mu = 5.29$ m/s, $\sigma = 0.3768$ m/s) than both single-joint ($\mu = 4.46$ m/s, $\sigma = 0.1706$ m/s) and zero-joint configurations ($\mu = 1.36$ m/s, $\sigma = 0.1097$ m/s). This study opens new avenues for the wing morphing design of unmanned aerial vehicles, offering the potential for achieving higher speeds while maintaining structural robustness.**

***Index Terms*—**

I. Introduction

Aerial engineering has continually evolved to increase the speed and stability of aircraft under various operational conditions. Current technological advancements have led to the implementation of variable-sweep wing systems, primarily characterized by a one-joint mechanism [1]. The surface area and sweep of aircraft wings are pivotal in enhancing diving speeds and managing aerodynamic forces, especially during rapid descent maneuvers. However, despite their efficacy, morphing wing designs often grapple with inherent limitations related to vibration management and mechanical stress during operation [2].

Birds are renowned for their aerial agility and efficiency, dynamically adjusting their wing shape and surface area to suit different flight conditions. For instance, bird wings can morph to increase lift and maneuverability during takeoff and landing, and streamline to reduce drag and conserve energy during cruising flight. Predator birds, such as falcons and hawks, exhibit a folding wing behavior during diving that has previously inspired aircraft design due to their aerodynamic shapes [3]. Inspired by the peregrine falcon, this project investigates a novel two-joint variable-sweep wing system. By emulating the natural wing morphing mechanisms of a peregrine falcon, this project aims to develop an aircraft with adaptable wing configurations capable of improving aerodynamic performance across a range of flight regimes [4].

Morphing wing technology highlights complex issues and gaps that require careful consideration in its design and implementation. There is a critical need for sophisticated control systems that maintain consistent stability and efficiency throughout the morphing process [5]. Additionally, actuation systems that combine high efficiency with powerful capability are critical, as they must support the changing aerodynamic shapes while keeping weight and energy use low. The major challenge is ensuring the aircraft's structure and skin are both durable and flexible enough to withstand significant shape changes for various flight scenarios without losing strength or adding unnecessary weight [6]. This creates a design dilemma, necessitating a balance between high stiffness for support and low stiffness for shape change, driving the exploration of innovative solutions like biomimetic fish bone structures, and designs featuring lattices and corrugations [4].

Despite progress in the area, fully incorporating morphing wing designs into the everyday operations of aircraft is still challenging. These challenges stem from difficulties in achieving the desired structural and aerodynamic performance, complexities in control systems, and the need for higher optimization and integrated system functionality [14]. The fact that many morphing wing ideas have not moved past the initial experimental stage highlights a substantial divide in applying these technologies to the industrial and commercial sectors, calling for focused research and development efforts to enhance the usability of morphing wing technology on a wider scale [11]. Recent research in bio-inspired aviation has delved into the aerodynamic properties of morphing wings. Stanford University's Lentink Lab introduced a biohybrid robotic platform featuring morphing wings, Pigeon Bot, to replicate the flexible flight capabilities of birds and analyze lift and drag in wind tunnel experiments [8]. Studies inspired by fish mechanics explore how morphing airfoil cross sections can create vortex wakes, showcasing potential applications for flying in challenging conditions [9]. However, limited research exists on morphing wing performance in extreme flight such as high-speed diving. Moreover, concerns persist regarding mechanical fatigue associated with complex, moving parts in morphing wing designs, with insufficient attention given to their implications for inducing structural vibrations compared to rigid wings [14]. Furthermore, addressing these concerns is imperative for the successful integration of morphing wing technology into future aircraft designs.

This study addresses a key gap in morphing wing technology by hypothesizing that a two-joint wing system, capable of

This work was funded by the Carnegie Mellon University Mechanical Engineering Department for the 24-775 Bioinspired Robot Design and Experimentation course.

folding its wings towards the body, can outperform traditional fixed-wing and one-joint configurations in terms of both diving speed and vibration suppression. This project has meaningful implications for the aerial robotics community and the aviation industry, as excessive vibration can lead to mechanical fatigue, shorten the lifespan of components, and risk failure at critical connections in the main rotor, engine, and battery power sources, ultimately influencing the reliability of the aircraft [10] [11]. Minimizing vibrations and increasing speed is anticipated to enhance the efficiency and dependability of aircraft, making a valuable contribution to the expansive domains of aerial robotics and aviation technology.

II. Design

To evaluate the hypothesis of this study, an aircraft was designed and manufactured, featuring a two-joint wing system capable of zero joint actuation (fixed wing), single joint actuation, and double joint actuation (see Figure 1). This design minimizes potential confounding variables that could arise from testing different wing configurations on separate aircraft. The design process commenced with the selection of the airfoil profile; the NACA 2412 was chosen for its prevalence in the field [15]. Such a profile is widely utilized in the aircraft industry and is supported by extensive real-world data, affirming its reliability. This profile was selected to ensure robust functionality in the wing design.

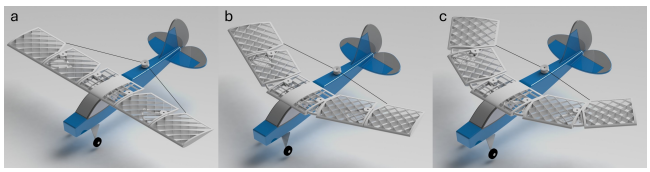

Fig. 1. CAD rendering of a) Zero Joint Actuation, b) Single Joint Actuation, and c) Double Joint Actuation.

The wing assembly is composed of five components: two outer wings, two inner wings, and one base that connects to the aircraft's body. To minimize weight, the base wing's infill is hollowed out and supplemented with vertical and horizontal ribs to enhance rigidity and counteract bending forces from lift. Unlike the base, both the outer and inner wings incorporate diagonal (45 degrees) cross rib designs. This configuration provides more comprehensive bending resistance at various angles, accommodating their capacity to sweep. Depicted in Figure C1, both the inner and outer wings feature 25-degree chamfers at their edges, oriented towards the fuselage and the rear of the aircraft. These chamfers come into contact with the base and inner wings at each stage of morphing, ensuring that the wings halt at a precise 25-degree angle during single joint actuation and at 50 degrees during double joint actuation.

The morphing capabilities of the aircraft are facilitated by two primary mechanisms: the joint mechanism and the spool mechanism. The joint mechanism, illustrated in Figure C2, employs quarter-circular shapes as guide rails for the rotational hinge motion. This quarter-circular shape is removed from one side of the inner wing and both sides of the base wing, allowing the quarter-circles to move within the wings and create friction to counteract bending from lift. The rotational axis of the circles is secured by a pin.

Additionally, a groove designed onto the quarter-circle hinge, shown in Figure C3, accommodates a torsion spring. This spring's body is anchored within the cylindrical slot, with one leg extending into a groove near the wing's edge. An extruded cut-out on the subtracted quarter-circle permits insertion of the spring's other leg. The holes for spring attachment are spaced 120 degrees apart on the inner wings and 110 degrees apart on the base wing, while the torsion spring itself is set at 90 degrees. This configuration places the spring under tension upon installation, generating torque to maintain the wings in the zero-degree actuation state.

The spool system incorporates a pulley linked to two strings (see Figure C4), each attached to the lower edge of the outer wings near the inner wings. This pulley is mounted atop the fuselage and connected to an FS90 motor positioned underneath. Activation of the motor causes the pulley to rotate, thereby tensioning the strings and drawing the outer wings towards the aircraft's rear. The pulley is strategically placed such that, at the double joint actuation stage, the two strings align collinearly, minimizing the torque load on the motor.

The design of the spring holes differs between the connections: 110 degrees for the base wing to the inner wing, and 120 degrees for the outer wing to the inner wing (Figure C1). Due to all torsion springs in the system having an identical spring rate, this arrangement results in a lower pretension torque between the base wing and the inner wing, yet it is sufficient to maintain the zero-degree actuation state without the spool system's intervention. When activated, the spool system initially causes rotation at the joints between the base wing and the inner wings, leading to single joint actuation. Further rotation of the pulley extends the outer wings backward, achieving double joint actuation. Reversing the pulley (spinning in the opposite direction) allows the torsion springs to exert torque, transitioning the wing system from double joint actuation to single, and then to zero joint actuation. This combination of spool and rotational mechanisms enables the aircraft to achieve all desired actuation with minimal components, significantly reducing the system's weight.

The wing assembly and pulley were fabricated using a Creality K1C 3D printer, utilizing FDM (Fused Deposition Modeling) 3D printing technology. eSUN PLA+ filament was selected for its combination of affordability and high strength. To enhance aerodynamic performance, the wings were covered with a transparent cellophane sheet.

The construction of the robot began with the disassembly of the wing from an RC plane. Subsequently, the fuselage was modified to accommodate the new wing assembly, with the base wing being securely affixed using hot glue. A hole was also cut into the fuselage to facilitate the connection of the pulley to the FS90 motor beneath. The pulley was then both glued and screwed onto the FS90 motor horn to ensure reliability. Finally, the strings were manually tightened to link the pulley with the outer wings, completing the setup.

III. Methods

A. Experimental Procedure

The experimental procedure for flight tests entailed throwing the glider from a consistent 130.5 inch height in the three wing configurations. Four team members held a blanket to capture the glider at the end of the dive. The blanket was held taut to maintain impact consistency. Following a delay of 2-3 seconds after the landing, the blanket was lowered. The next step involved measuring the horizontal distance from the launch site, followed by a waiting period of 2-3 minutes for the SD card to log the data. Finally, video data was logged to complete the procedure. This procedure was repeated 5 times for each wing configuration, for a total of 15 trials. Motion capture techniques were then employed, utilizing Tracker Video Analysis and Modeling Tool software to derive positional data for velocity calculation. Finally, data analysis was performed utilizing Excel, Python, and MATLAB, where video flight time stamps were synchronized with altimeter data to extract diving duration.

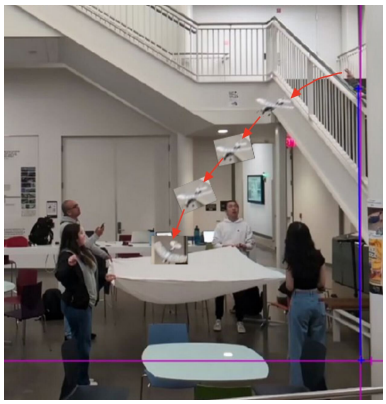

Fig. 2. Gliding Experimentation Setup and Motion Capture

B. Tracker Motion Analysis

Tracker is a video analysis and modeling tool built on the Open Source Physics Java framework. It collects velocity data from videos processed using Tracker. The Tracker features allows for complete manual object tracking with position, velocity, and acceleration overlays and data, center of mass tracks, manual calibration, and diving angle collection. By setting origins and consistent height of the gliding test using the calibration stick function, it sets up the distance systems for the experimentation data collection. Point mass motion capture for each point for precise analysis of gliding trajectory. MATLAB was used to plot the data collected from Tracker. Additionally, The timeframe from the video was precisely tracked in Tracker and used for vibration data anaylsis to match with each timestep for the vibration results.

C. Altitude-Based Data Processing and Analysis:

Along with using Tracker, the team performed an analysis based on altimeter sensor (BMP390) data, which tracked the aircraft's sea level altitude. The sensor demonstrated high accuracy, with deviations of 1-3 meters from the true sea level of the testing location. Altitude and vibration 1 and 2 data were collected every 5 milliseconds (up to 4000 milliseconds) using an Arduino Nano, which logged the data onto a MicroSD card reader, powered by a 9V power source. Data logging lasted around two minutes, and the altitude plots showed consistent descent during the trials, aligning with the measured height difference of 3.3 meters.

The altitude descent data was correlated with the vibration data for a real-time sensor-based analysis. The raw altitude data was inspected for continuous negative gradient intervals and filtered, then used to index into vibrations 1 and 2. Horizontal displacement and flight times were scaled accordingly. Velocity was calculated from the resultant vertical and horizontal displacement components.

During descent, there was a dip of 2-3 meters, with minimal noise, captured accurately through the gradient method. The sensor indicated flight times of 50 to 200 milliseconds, while Tracker recorded around 1 second. The sensor time scale was re-aligned with Tracker, resulting in accurate horizontal and vertical time series data and velocities for each sample.

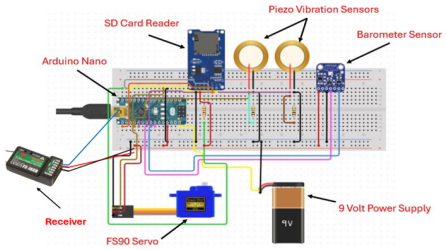

Fig. 3. Schematic of electronics that were carefully placed in fuselage

D. Electronics and Sensors

The onboard electronics consist of two piezo-vibration sensors, a BMP390 barometer sensor, and SD Card reader (with a 16 MB SD card), and FS90 servo. These were all connected to an Arduino Nano via Analog and I2C protocol communication. Additionally, an FS-IA6B receiver was integrated for remote servo commands. The entire circuit was provided with 9V external power, which satisfied our current draw needs. The electronics schematic is pictured in Figure 3.

IV. Results

This project employed two approaches for analyzing the flight dynamics of the aircraft: video analysis using the Tracker software and sensor-based altitude data processing.

A. Tracker-based Results

The Tracker software facilitated detailed video-based motion analysis. This tool allowed for tracking of the position, velocity, and acceleration of the aircraft. The calibration feature ensured consistent height measurements across gliding tests, using a calibration stick to set the distance system for data collection. Through this method, insights were obtained into the aircraft's dynamics during various joint actuation.

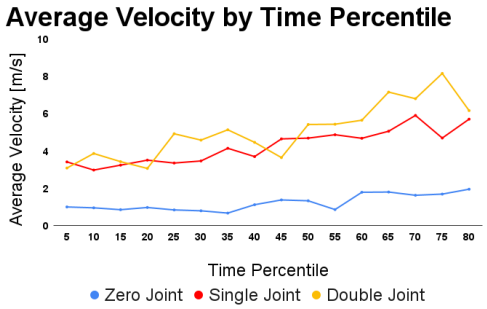

Fig. 4. The average velocities were calculated at the same time percentile to reduce the standard deviation of the velocities averaged over the entire diving duration.

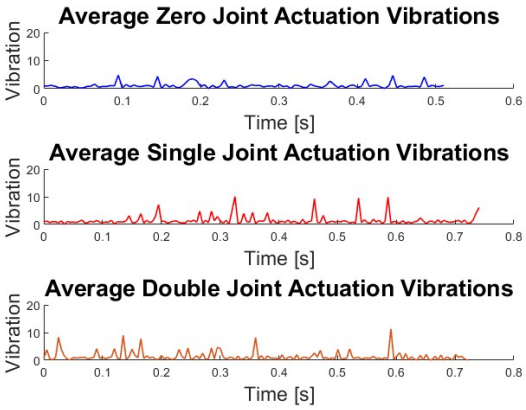

Fig. 5. The average vibrations were plotted during the duration of diving flight. Diving duration was found through the time stamps of each video.

The velocity and vibration profiles for zero-joint, single-joint, and double-joint actuation demonstrated variation, as shown in Figures 4 and 5.

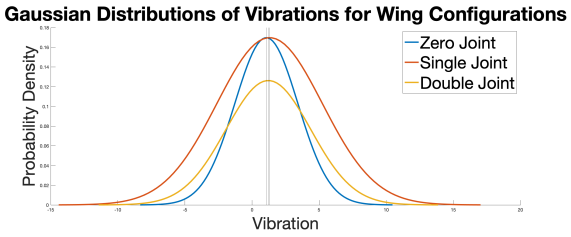

Fig. 6. Gaussian distributions of vibrations for all wing configurations. Distribution parameters were calculated from a sample size of 865.

Table 1: Distribution Parameters and T-test for Wing Vibrations

Group	Mean	SD	Group	p-value
Zero Joint (Z)	0.9548	1.9944	$\mu_D > \mu_Z$	0.0398
Single Joint (S)	1.3088	3.9298	$\mu_S > \mu_Z$	0.0183
Double Joint (D)	1.2162	3.1609	$\mu_D > \mu_S$	0.5893

The Gaussian distributions of velocities for the different wing configurations, illustrated in Figure 7, show distinct

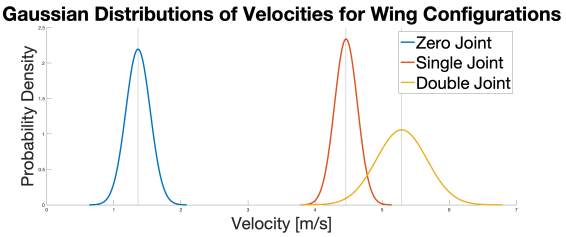

Fig. 7. Gaussian distributions of velocities for all wing configurations. Distribution parameters were calculated from a sample size of 5.

Table 2: Distribution Parameters and T-Test for Velocities [m/s]

Group	Mean	SD	Group	p-value
Zero Joint (Z)	1.36	0.1097	$\mu_D > \mu_Z$	5.974e-7
Single Joint (S)	4.46	0.1706	$\mu_S > \mu_Z$	1.549e-8
Double Joint (D)	5.29	0.3768	$\mu_D > \mu_S$	0.0049

peaks, indicating that double-joint wings achieve the highest average velocities, followed by single-joint and zero-joint configurations.

Similarly, the Gaussian distributions of vibrations for all wing configurations, illustrated in Figure 6, reveal that the double-joint and single-joint wings exhibit higher vibrations than the zero-joint configuration.

The statistical analysis presented in Table 1 and Table 2 support these findings, with the t-test results showing a significant difference in vibration levels between the zero-joint and single-joint configurations ($\mu_S > \mu_Z$) and between the zero-joint and double-joint configurations ($\mu_D > \mu_Z$). However, there is no significant difference between the single-joint and double-joint configurations ($\mu_D = \mu_S$). There is statistically significant differences in velocities across all wing configurations, where the double-joint configuration has higher velocities than both single-joint and zero-joint configurations ($\mu_D > \mu_S > \mu_Z$).

B. Altitude-based Results

After data processing, 5 vibration 1, 5 vibration 2 samples and five velocity samples from each category were averaged. To determine if the data was normally distributed for Gaussian analysis, the D'Agostino's K-squared test was performed on each averaged dataset. These resulted in non-normal distributed results for each averaged dataset for vibrations 1, 2 and velocities. To avoid misleading inferences and outlier sensitivity, the non-parametric Mann-Whitney U testwas used, which operates on ranking observations on groups rather than raw data values. For Vibration 1, the p-values between zero/double-joint, zero/single-joint were greater than 0.05. However, between single/double-joint, a p-value of 0.01 was obtained, implying a statistical difference between those datasets. For Vibration 2, the p-values between zero/double-joint were greater than 0.05. However, between zero/single and single/double, the p-values of 0.01 were obtained, implying a statistical difference between those datasets. Based on the common difference between Single-Double datasets, the vibration hypothesis can be limited to these two joint configurations.

When comparing average velocities, the p-values are greater than 0.05 suggesting no statistical difference between diving speeds in any configuration, disproving the speed hypothesis. After, an Fast-Fourier was applied to each dataset, where vibration amplitudes were obsered to reduce from 28.4 & 24.1 (single) to 17.23 & 18.1 (double).

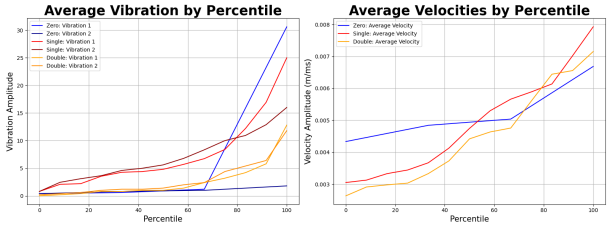

Fig. 8. Altitude-Based: Average Vibrations and Velocities.

Table 3: Mann-Whitney U test for Wing Vibrations

Group	Mean	SD	Group	p-value
Zero Joint: Vib 1,2	8.2, 1.0	12.9, 0.5	S_D&S_Z	1.0, 0.23
Single Joint: Vib 1,2	7.5, 6.9	6.7, 4.3	S_S&S_Z	0.2, 0.01
Double Joint: Vib 1,2	2.6, 3.0	3.4, 3.2	S_D&S_S	0.01

Table 4: Mann-Whitney U test for Average Velocities (m/ms)

Group	Mean	SD	Group	p-value
Zero Joint: Vib 1,2	0.004	0.001	S_D&S_Z	0.29
Single Joint: Vib 1,2	0.004	0.001	S_S&S_Z	0.77
Double Joint: Vib 1,2	0.005	0.0008	S_D&S_S	0.43

Table 5: Vibration FFT Results

	Peak Freq (Hz)	Peak Amplitude
Zero Joint: Vibrations 1,2	0.003, 0.003	30.2, 1.41
Single Joint: Vibrations 1,2	0.006, 0.004	28.4, 24.1
Double Joint: Vibrations 1,2	0.001, 0.001	17.23, 18.1

V. Conclusions

The outcomes of the one-tailed unpaired t-test from Tracker data reveal trends in both vibration and speed dynamics among different wing configurations. The hypothesis that double-joint wings exhibit higher velocities was supported, as double-jointed wings showed the highest average velocities, followed by single-joint wings, and then zero-joint wings. However, the hypothesis that double-joint wings have lower vibrations was not supported. Specifically, the analysis indicates that vibrations follow a hierarchical pattern, with double-joint wings exhibiting the highest levels, followed by single-joint wings, and then zero-joint wings. While there exists no statistically significant difference between the vibration levels of variable-sweep wings, it is noteworthy that both configurations demonstrate higher average vibrations compared to fixed wings. This observation underscores the potential importance of jointed structures in mitigating the vibration effects during flight.

For the altimeter-based study, the Mann-Whitney U test, for non-normally distributed data, was applied to the processed data, where there were complete statistical differences between single and double-joint vibrations, with a partial difference for the vibration 2 sensor between zero and single-joint. By limiting the comparison between single and double-joint, vibrations are observed to reduce in FFT from single to double in the FFT results. Also, lower vibrations in double-joint percentiles were obtained, as according to Figure 8. This study proves but limits the hypothesis to reduce vibrations between single and double-joint wing configurations, but rules inconclusive for diving velocities.

Future work should focus on calibrating the altimeter and vibration sensor noise and investigating time delay noise to improve real-time recording accuracy. More consistent flight testing trials may be achieved by creating a launch pad or ramp to control trajectory entry angle and velocity. Additionally, it may be beneficial to implement an Inertial Measurement Unit (IMU) to track possible rotation during flight, verify position using integration and filtering methods, and further enhance the understanding of double-joint wing efficiency.

References

[1] Z. Gao, Y. Luo, Z. Luo, and Y. Zhao, "Design and Analysis of a Variable-sweep Morphing Wing for UAV Applications," in 2021 IEEE International Conference on Robotics and Biomimetics (ROBIO), 2021, pp. 1–6, doi: 10.1109/ROBIO54168.2021.9739269.

[2] A. Prabhakar and R. J. Prazenica, "Design and Dynamic Analysis of a Variable-Sweep, Variable-Span Morphing Wing for UAV Applications," Embry-Riddle Aeronautical University, 2015.

[3] J. Han, Z. Hui, F. Tian, and G. Chen, "Review on bio-inspired flight systems and bionic aerodynamics," *Chinese Journal of Aeronautics*, Jun. 2020, doi: https://doi.org/10.1016/j.cja.2020.03.036.

[4] Li, D., Zhao, S., Da Ronch, A., Xiang, J., Drofelnik, J., Li, Y., Zhang, L., Wu, Y., Kintscher, M., Monner, H. P., Rudenko, A., Guo, S., Yin, W., Kirn, J., Storm, S., & Breuker, R. D. (2018a). A review of modelling and analysis of Morphing Wings. *Progress in Aerospace Sciences*, 100, 46–62, doi: https://doi.org/10.1016/j.paerosci.2018.06.002.

[5] Martins, J. R. (2022). Aerodynamic design optimization: Challenges and perspectives. Aerospace Science and Technology, 123, 107524.

[6] J. Zhu, J. Yang, W. Zhang, and Y. Xu, "Design and applications of morphing aircraft and their structures," Frontiers of Mechanical Engineering, vol. 18, pp. 34, 2023, doi: 10.1007/s11465-023-0750-6.

[7] Zhu, J., Yang, J., Zhang, W., Gu, X., & Zhou, H. (2023). Design and applications of morphing aircraft and their structures. *Frontiers of Mechanical Engineering*, 18(3), doi: https://doi.org/10.1007/s11465-023-0750-6.

[8] E. Chang, L. Y. Matloff, A. K. Stowers, and D. Lentink, "Soft biohybrid morphing wings with feathers underactuated by wrist and finger motion," *Science Robotics*, vol. 5, no. 38, Jan. 2020, doi: https://doi.org/10.1126/scirobotics.aay1246.

[9] B. K. S. Woods, L. Parsons, A. B. Coles, J. H. S. Fincham, and M. I. Friswell, "Morphing elastically lofted transition for active camber control surfaces," *Aerospace Science and Technology*, vol. 55, pp. 439–448, Aug. 2016, doi: https://doi.org/10.1016/j.ast.2016.06.017.

[10] M. Abdulrahman Al-Mashhadani, "Random vibrations in unmanned aerial vehicles, mathematical analysis and control methodology based on expectation and probability," *Journal of Low Frequency Noise, Vibration and Active Control*, vol. 38, no. 1, pp. 143–153, Dec. 2018, doi: https://doi.org/10.1177/1461348418813031.

[11] K. Chen, W. Meng, J. Wang, K. Liu, and Z. Lu, "An investigation on the structural vibrations of multi-rotor passenger drones," *International Journal of Micro Air Vehicles*, vol. 15, Jan. 2023, doi: https://doi.org/10.1177/17568293231199097.

[12] J. R. Usherwood, M. Stavrou, J. C. Lowe, K. Roskilly, and A. M. Wilson, "Experimental evidence for the aerodynamic function of tail feathers in birds," *Journal of Experimental Biology*, vol. 214, no. 20, pp. 3410-3418, 2011.

[13] Agarwal, R. K. (2024). Grand challenges in aerospace engineering. *Frontiers in Aerospace Engineering*, 3, 1383934. doi: 10.3389/fpace.2024.1383934.

[14] Barbarino, S., Bilgen, O., Ajaj, R. M., Friswell, M. I., & Inman, D. J. (2011). A review of morphing aircraft. Journal of Intelligent Material Systems and Structures, 22(9), 823-877.

[15] NACA 2412 (NACA2412-IL), "NACA 2412 Airfoil," http://airfoiltools.com/airfoil/details?airfoil=naca2412-il, accessed May 05, 2024.

APPENDIX

A. Individual Technical Contributions

Jonathan Ali -
Jonathan spearheaded the electronics design and sensor data logging framework for the aircraft. His role encompassed research into sensor technologies that would be viable for data analysis. Jonathan's role included selecting, assembling and experimenting sensors with various microcontroller platforms, ensuring seamless compatibility and optimal performance. He delved into optimizing power management and current draw requirements for the electronics subsystem, while addressing potential pitfalls in upholding the reliability and efficiency of the flight data collection process. Beyond hardware integration, he led the charge in refining data reading techniques, exploring and visualizing critical flight metrics such as altitude and vibration, employing advanced algorithms for accurate interpretation. In addition, Jonathan performed vibrational analysis through FFT (Fast Fourier Transform) techniques, offering insights into the aircraft's structural dynamics. He was also responsible for rectifying data timestamps and curating measurements from trial runs.

Karla Soto Cuevas -
Karla focused on the radio control and wing morphing mechanism of the aircraft. She identified electronics and analyzed power needs for the wing sweep mechanism, integrated actuators into the first prototypes, and programmed the radio controls in Arduino. She conducted fixed-wing flight tests, using Tracker software to capture motion data, and normalized speed data for varying diving angles. Karla configured the FS-i6 transmitter and receiver system, tested positional servo motors, and addressed limited motor turning angles by extending servo operating angles to 180 degrees using Arduino code. She incorporated continuous rotation servo motors, refined PWM signals, and assessed performance with a string-pulley system. Additionally, Karla captured velocity data from flight test videos using Tracker, matched velocity data from the motion capture analysis with onboard altimeter sensors for validation, and conducted t-tests on vibrations and velocities across test groups.

Kruti Rachapudi -
Kruti worked on the design and prototyping of the robotic glider as well as management of the groups schedule and budget. Kruti refined the research hypothesis to better suit the project's needs after the proposal. She made updates to the team Gantt chart and assigned tasks to team members, including selecting and ordering components like foam for wings or the RC plane. For the design of the wing, Kruti researched torsion spring assemblies and implemented in the CAD. After an initial 3D print of the wing, Kruti conferred with Professor Webster-Wood regarding feasibility concerns, leading to a redesign of the wing prototype aimed at maximizing lightness. This involved adopting a skeletal structure and removing non-essential sections to reduce weight. As Tommii took over the wing design, Kruti transitioned to experimentation. She found the optimal experimental set up and launched the plane for each of the trials. The data collected by the vibration sensors were averaged by Kruti using the time intervals of diving that Karla provided.

Helen Wang -
Helen focused on the development of the landing gear system, from CAD design to prototyping, ensuring its functionality and reliability in the test rig demonstration. She conducted thorough electronics testing and research, exploring the capabilities of the chosen components, such as the Piezo ceramics vibration sensor's testing and calibration on its unit setup. She designed and constructed a comprehensive test rig with aluminum extrusion and maple wood to demonstrate the morphological capabilities of the bird-inspired aerial robot, showcasing its fuselage, morph wing, and landing capabilities. She collaborated with the team to prototype the wing sweep mechanism and spool mechanism, and installed them onto the fuselage. Throughout the experimentation process, she conducted motion capture data analysis through Tracker video analysis and modeling tool software to derive positional data for velocity calculation.

Tommii Zeng -
Tommii led the design and fabrication efforts for the project, translating the team's ideas into functional CAD models using SOLIDWORKS. At the start of the semester, he developed an initial conceptual design, introducing quarter-circle rotational mechanisms that facilitated the two joint morphing wing concept. He completed the prototype design, integrating all necessary electronic components and stabilizers, and produced several 3D-printed iterations for testing. In the latter half of the semester, following Kruti's recommendations, Tommii spearheaded the redesign of the aircraft to incorporate the existing wing design into an RC plane, with an emphasis on weight reduction. He worked collaboratively to embed the torsion springs and spool mechanisms into the final robot design and carried out extensive testing to refine the working prototypes. Tommii managed the assembly and disassembly processes during the experimental phases, actively participated in the collection of experimentation videos, and assisted in constructing the demo rig for the Expo.

B. Budget

	Part #	Source	Every Day Price	Qty.	Running Totals
compression springs	1	Amazon	$8.91	1	$8.91
torsional springs	2	McMaster	$7.25	1	$7.25
foams	3	Amazon	$14.39	1	$14.39
servo motors	4	TechSpark	$4.00	7	$28.00
foam cutter	5	Amazon	$21.69	1	$21.69
Vibration Sensor	6	Amazon	$6.99	1	$6.99
6-axis Accelerometer Gyroscope Sensor	7	Amazon	$9.99	1	$9.99
Dynamixel AX-12A	8	Class	$24.95	1	$24.95
DC Motor w/Propeller	9	Amazon	$21.99	1	$21.99
elastomeric wheels	10	Amazon	$9.59	1	$9.59
new vibration sensors (force sensor)	11	Sparkfun	$7.50	1	$7.50
SG90 servo motor	12	TechSpark	$3.00	4	$12.00
RC plane	13	Amazon	$159.99	1	$159.99
FS-i6 Tranmistter + FS-ia10b Recevier	14	Amazon	$59.99	1	$59.99
FS-ia10b Receiver	15	Amazon	$19.87	1	$19.87
Corona Servo	16		$12.28	1	$12.28
Torsonial Spring	17	McMaster	$6.51	1	$6.51
GPS Module	18	Amazon	$8.99	2	$17.98
4pcs 400mm T Slot 2020 Aluminum Extrusion	19	Amazon	$18.99	1	$18.99
12pcs 20mm Open Gussets Corner Brackets	20	Amazon	$9.99	1	$9.99
4pcs 53mm corner brackets	21	Amazon	$15.99	1	$15.99
SD Card	22	Amazon	$7.49	1	$7.49
SD Card Reader	23	Amazon	$11.42	1	$11.42
ESP32	24	Amazon	$9.99	1	$9.99
Altimeter/Barometer	25	Amazon	$14.99	1	$14.99
AAA battery for control	26	TechSpark	$2	1	$2
battery holder	27	TechSpark	$2	1	$2
RC plane	28	Amazon	$159.99	1	$159.99
eSUN PLA+ Filament (Cold White)	29	Amazon	$16.99	2	$33.98
Arduino Nano	30	Amazon	$9.99	1	$9.99
ESP32	31	Amazon	$9.99	1	$9.99
Junction Connectors	32	Amazon	$9.99	1	$9.99
Hinge for test rig	33	Amazon	$8.99	1	$8.99
Orientation Sensor	34	Amazon	$14.99	1	$14.99
FG90 Servos	35	Amazon	$28.61	1	$28.61
				Current Total	$819.26
				Leftover Budget	$180.74

Fig. B1. Purchasing List for the project

C. Figures

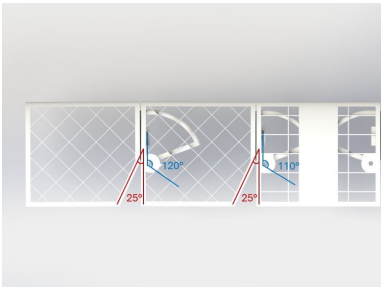

Fig. C1. Left wing assembly with outer wing (left), inner wing (middle), and base wing (right). Chamfer angles (red) and spring groove and hole angles (blue) are shown.

Fig. C2. Explosion view of the joint mechanism consisting the inner (left), the base wing (right), and the torsion spring.

Fig. C3. Torsion spring groove (top) and hole (right).

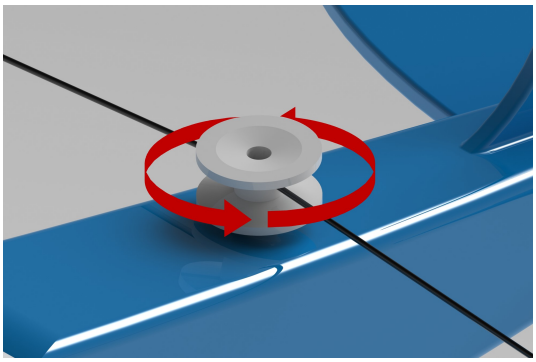

Fig. C4. Spool mechanism, the pulley (white) and two strings (black), and its direction of motion.

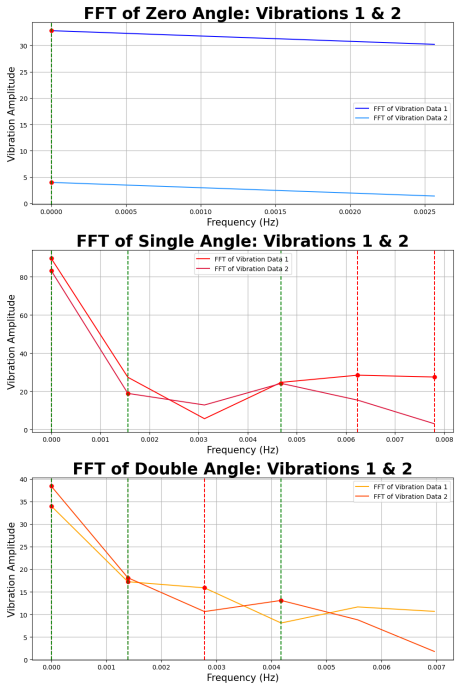

Fig. C5. Fast-Fourier Transform (FFT) of zero-, single- and double-joint configurations. Each plot shows the top three peak amplitudes of vibration. The second frequency and amplitude was analyzed from each plot to avoid zero frequencies which report the average value of the signal.